Homoclinic orbits around spinning black holes. I. Exact solution for the Kerr separatrix

Janna Levin[1,2,*] and Gabe Perez-Giz[3,†]

[1]*Department of Physics and Astronomy, Barnard College of Columbia University, 3009 Broadway, New York, New York 10027, USA*
[2]*Institute for Strings, Cosmology and Astroparticle Physics, Columbia University, New York, New York 10027, USA*
[3]*Physics Department, Columbia University, New York, New York 10027, USA*

For equatorial Kerr orbits, we show that each separatrix between bound and plunging geodesics is a homoclinic orbit—an orbit that asymptotes to an energetically-bound, unstable circular orbit. We derive exact expressions for these trajectories in terms of elementary functions. We also clarify the formal connection between the separatrix and zoom-whirl orbits and show that, contrary to popular belief, zoom-whirl behavior is not intrinsically a near-separatrix phenomenon. This paper focuses on homoclinic behavior in physical space, while in a companion paper we paint the complementary phase space portrait. Although they refer to geodesic motion, the exact solutions for the Kerr separatrix could be useful for analytic or numerical studies of eccentric transitions from orbital to plunging motion under the dissipative effects of gravitational radiation.

I. INTRODUCTION

A. Background and motivation

A direct observational detection of gravitational waves—perhaps the most fundamental prediction of a theory of curved spacetime—looms close at hand. Stellar mass compact objects spiraling into supermassive black holes have received particular attention as sources of gravitational radiation for the planned LISA mission [1]. A direct detection of these extreme mass ratio inspirals (EMRIs), as well as extraction of astrophysics [2–7], requires a thorough knowledge of the underlying dynamics; it is the motion of the two bodies that shapes the gravitational waveform. A well-established approach models the EMRI as an adiabatic progression through a series of Kerr geodesics [3–9]. A transparent depiction of geodesic motion around spinning black holes is therefore essential yet seemingly complicated [10,11] and benefits from crucial signposts in the orbital dynamics.

We decipher such a crucial signpost here. In particular, we discuss an important family of separatrices in Kerr dynamics: the homoclinic orbits. Around black holes, the homoclinic orbits are those that asymptotically approach the same unstable circular orbit in both the infinite future and the infinite past,[1] as shown on the right of Fig. 1. Under the identifier ''separatrix,'' homoclinic orbits have already garnered attention in the black hole literature [12,13]—the homoclinic orbit is the separatrix between orbits that plunge to the horizon and those that do not.[2] The scenario of quasicircular inspiral through a last stable circular orbit is a special example of the transition through a zero eccentricity homoclinic orbit. To the extent that adiabatic evolution is valid, orbits that merge before they have a chance to circularize will transit through an eccentric homoclinic orbit of the underlying conservative dynamics. Any analysis of the transition from inspiral to plunge will thus run into this special family.

Homoclinic orbits are also a significant signpost for zoom-whirl behavior, an extreme form of perihelion precession wherein trajectories zoom out into quasielliptical leaves en route to apastron and then execute multiple quasicircular whirls near periastron before zooming out again, as shown in the left panel of Fig. 1. Though zoom-whirl behavior is sometimes thought to be associated only with highly eccentric orbits near the separatrix, we developed a topological criterion for whirliness in [11] and showed that in the strong-field regime, zoom-whirliness can appear for Kerr test particle orbits[3] at any eccentricity. Indeed, zoom-whirl behavior is neither exotic nor rare for test particle motion in the strong field [11]. Still, homoclinic orbits are relevant as an infinite whirl limit in the distribution of geodesics, a connection we forge in this paper.

Homoclinic orbits are therefore significant in shaping the geography of black hole orbits. In this first paper in a two part series, we devote some labor to resolving this landmark in physical space for equatorial orbits. (We leave for a future work the nonequatorial case.) The pinnacle is

---

*janna@astro.columbia.edu
†gabe@phys.columbia.edu
[1]Orbits that approach two different orbits in the infinite future and past, in contrast, are called *heteroclinic orbits*.
[2]The terms ''homoclinic orbit'' and separatrix are, in this context, entirely interchangeable, although the former finds more use in the dynamical systems literature and the latter in the black hole and gravitational wave literature.

[3]Reference [11] treated test particle geodesics only—the extreme mass ratio limit in the absence of radiation reaction. References [14,15] found zoom-whirl behavior in the post-Newtonian approximation, also in the absence of radiation, for other mass ratios. What distribution of zoom-whirl orbits at various eccentricities full numerical relativity simulations might be able to observe is an open question.
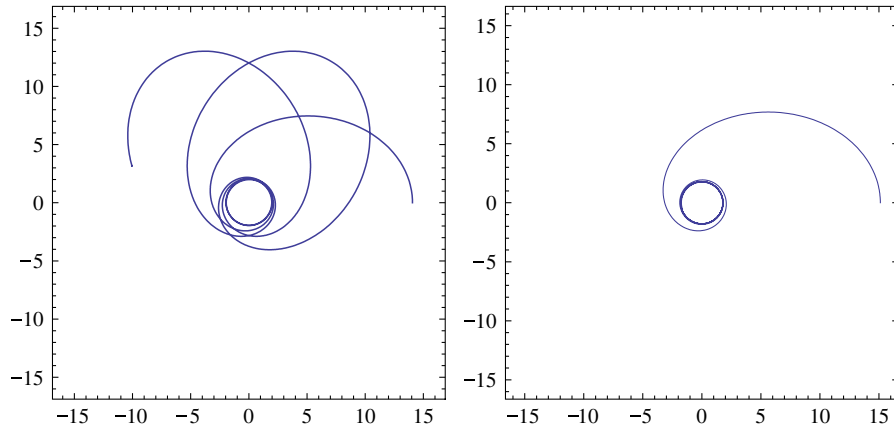
FIG. 1 (color online). Left: A zoom-whirl orbit. Right: A homoclinic orbit approaching an unstable circular orbit.

an exact solution for equatorial homoclinic trajectories. A rarity among relativistic orbits, the exact solution can make semianalytic treatment of the eccentric transition to plunge more wieldy. In paper II [16], we describe the flipside of the coin and detail the phase space portrait of the homoclinic orbits. We hope the results will provide cohesion to the dynamical conversation.

We begin this paper by finding exact expressions for the orbital parameters of the separatrices and use them to derive Eqs. (26), exact expressions for the trajectories themselves. As this paper is concerned with the physical space portrait of homoclinic orbits, we include a final section summarizing the generality of zoom-whirl behavior and where the separatrix fits in the spectrum of zoom-whirl orbits.

B. Homoclinic orbits in the gravitational wave literature

For context, we note that homoclinic orbits have appeared in the gravitational wave literature, although not always identified by name. Reference [12] analyzed the transition for equatorial eccentric Kerr orbits using semi-analytic methods. Gravitational wave snapshots and semi-analytic estimates of the radiative evolution of orbits near the separatrix appear in [13], which also discusses the "zoom-whirl" behavior that may be visible during an eccentric transition to plunge. The discussion of separatri-ces and their role in eccentric transitions to plunge is also being discussed for comparable mass systems [14,17], and an eccentric transition to plunge, including visible zoom-whirl behavior, has been observed in a full numerical relativity simulation of the merger of equal mass black holes [18].

Homoclinic orbits have also been discussed by name in the black hole literature and are not unique to extreme mass ratio binaries. The distinct imprint on a gravitational wave-form from the whirl phases or orbits near the homoclinic set was discussed in [19] for both Schwarzschild orbits and

orbits generated in the post-Newtonian (PN) expansion. A program to identify the homoclinic orbits in a higher-order PN expansion is also underway [14]. Reference [20] pro-vides a nice summary of the interesting phenomenology associated with homoclinic orbits in any dynamical sys-tem, and for the case of Schwarzschild geodesics formally demonstrates (using a somewhat unphysical example) the onset of chaos[4] around the homoclinic orbits when the system is slightly perturbed from the conservative dynam-ics, a fact that could be important in the analysis of the transition to plunge but which we do not discuss further here.

While homoclinic orbits are present even in comparable mass black hole systems described in a PN expansion, the complexity of the PN equations of motion makes analytic results about homoclinic orbits difficult to come by for comparable mass systems [15]. Since most of those refer-ences compare results against the Kerr equatorial case, we restrict our attention here to the fiducial case of homoclinic orbits in the equatorial plane of Kerr black holes.

II. ORBITAL PARAMETERS OF HOMOCLINIC ORBITS

The equatorial homoclinic Kerr orbits asymptotically approach the same unstable circular orbit in the infinite future and past, whirling an infinite number of times as they do so. In this section, we provide the afore-promised formal definition of a homoclinic orbit and substantiate this claim.

A. Definition of a homoclinic orbit

Formally, a homoclinic orbit approaches the same in-variant set in the infinite future as in the infinite past. A

---

[4]Small perturbations to the entire system give rise to structures in the phase space, first discussed by Poincare [21] and usually termed "homoclinic tangles," that are quantifiable signatures of chaos.

collection of points S in the phase space of a dynamical system is an invariant set if orbits that are in the set at any time remain in the set for all previous and subsequent times. Of course, the set of points in phase space traced out by any solution to the equations of motion constitutes an invariant set, but useful information about global properties of the phase space usually comes from identifying invariant sets with some associated *recurrence property*, such as fixed points, periodic orbits, or the n-dimensional tori on which bounded quasiperiodic motion in integrable systems unfolds. Henceforth, when we refer to an invariant set, we will always mean a recurrent invariant set.

The set of all trajectories that approach S asymptotically in the infinite future is a submanifold of the phase space, namely, the stable manifold of S. Likewise, all trajectories that approach S asymptotically in the infinite past form the unstable manifold of S. An invariant set is called hyperbolic if it has both a stable and an unstable manifold.

Now, stable and unstable manifolds of invariant sets can sometimes intersect: some individual trajectories may approach (possibly different) invariant sets both as $t \to +\infty$ and as $t \to -\infty$. When such a trajectory lies in the stable manifold of one invariant set S_+ and the unstable manifold of a different invariant set S_-, the trajectory is heteroclinic to S_+ and S_-. If instead the trajectory approaches the same invariant set S in the infinite future and past, i.e. if it is an intersection of the stable and unstable manifolds of *the same set S*, then the trajectory is homoclinic to S.

Identifying the homoclinic orbits in a dynamical system thus amounts to finding the intersections of the stable and unstable manifolds of its hyperbolic invariant sets. As we will now show, for the system of Kerr equatorial orbits, the only hyperbolic invariant sets with associated homoclinic orbits are the energetically bounded, unstable circular orbits. Strictly speaking, no relativistic orbits are truly recurrent since time itself is a coordinate in a relativistic phase space [22,23] and all orbits are unbounded in their forward motion in time. We will go to some trouble in paper II [16] to reduce to a 6D phase space of spatial coordinates and their conjugate momenta in which circular orbits are truly recurrent invariant sets.

B. Kerr equations of motion

The Kerr metric in Boyer-Lindquist coordinates and geometrized units ($G = c = 1$) is

$$ds^2 = -\left(1 - \frac{2Mr}{\Sigma}\right)dt^2 - \frac{4Mar\sin^2\theta}{\Sigma}dtd\varphi$$

$$+ \sin^2\theta\left(r^2 + a^2 + \frac{2Ma^2r\sin^2\theta}{\Sigma}\right)d\varphi^2 + \frac{\Sigma}{\Delta}dr^2$$

$$+ \Sigma d\theta^2, \tag{1}$$

where M, a denote the central black hole mass and spin angular momentum per unit mass, respectively, and

$$\Sigma \equiv r^2 + a^2\cos^2\theta \qquad \Delta \equiv r^2 - 2Mr + a^2. \tag{2}$$

Motion along geodesics of (1) conserves orbital energy E, axial angular momentum L_z, the Carter constant Q [24], and of course the rest mass μ of the test particle itself.[5] Since there are as many constants of motion as degrees of freedom, the usually second order geodesic equations can be integrated to yield a set of 4 first-order equations of motion for the coordinates [24]. Before writing them down, we adopt the useful and now common convention [22] to set both M and μ equal to 1, an operation tantamount to working in units in which the coordinates r and t, the proper time τ, the spin parameter a and the conserved quantities E, L_z, Q are all dimensionless. In these dimensionless units, which we use in the remainder of this paper, the first-order geodesic equations are

$$\Sigma\dot{r} = \pm\sqrt{R} \tag{3a}$$

$$\Sigma\dot{\theta} = \pm\sqrt{\Theta} \tag{3b}$$

$$\Sigma\dot{\varphi} = \frac{a}{\Delta}(2rE - aL_z) + \frac{L_z}{\sin^2\theta} \tag{3c}$$

$$\Sigma\dot{t} = \frac{(r^2 + a^2)^2E - 2arL_z}{\Delta} - a^2E\sin^2\theta, \tag{3d}$$

where an overdot denotes differentiation with respect to the particle's (dimensionless) proper time τ and

$$\Theta(\theta) = Q - \cos^2\theta\left\{a^2(1 - E^2) + \frac{L_z^2}{\sin^2\theta}\right\} \tag{4}$$

$$R(r) = -(1 - E^2)r^4 + 2r^3 - [a^2(1 - E^2) + L_z^2]r^2$$

$$+ 2(aE - L_z)^2r - Q\Delta. \tag{5}$$

Modulo initial conditions, we can identify any orbit around a black hole of some mass and spin by its constants of motion E, L_z and Q. From this point on, we will restrict attention to equatorial orbits. Equatorial Kerr orbits have $\theta = \pi/2$ and $\dot{\theta} = 0$. It follows from the equations of motion (3) that equatorial orbits always have $Q = 0$ and that they remain equatorial and form a self-contained set.

In the following section we will identify the homoclinic orbits with the aid of an effective potential picture.

C. Effective potential and the homoclinic orbits

To clarify terms, it is standard parlance to refer to "unstable" circular orbits in the black hole system. Strictly speaking, the unstable circular orbits are actually hyperbolic—they possess both a stable and unstable mani-

---

[5]E and L_z are associated with t-translation and φ-translation Killing vectors of the Kerr metric. Q is associated with a Killing tensor with a less obvious geometric interpretation. In the weak field, $Q \approx L_x^2 + L_y^2$

fold. Nonetheless, we continue with this conventional parlance to avoid unnecessarily elaborate verbiage and assume the reader understands phrasing such as "the stable manifold of an unstable circular orbit."

The hyperbolic invariant sets in the equatorial Kerr system are precisely these unstable circular orbits. Of those, the ones that are energetically bound ($E < 1$) give rise to homoclinic orbits.

Identification of the homoclinic orbits, and indeed interpretation of the dynamics in general, is easiest with an effective potential formulation, which motion around spinning black holes admits. However, as we explain shortly, the Kerr effective potential has some awkward features that make our exposition a bit cumbersome. Thus, to ease discussion, we briefly recount the effective potential picture for Schwarzschild black holes [20,25–27] and identify the homoclinic orbits for that case before extending to Kerr black holes. This subsection amounts to a synopsis of the familiar specifics of orbits admitted by the Schwarzschild and Kerr effective potentials, a lengthier accounting of which we include in Appendix A for the detail conscious reader.

For Schwarzschild orbits ($a = 0$), the suggestive form

$$\frac{1}{2}\dot{r}^2 - \frac{R(r)}{2\Sigma^2} = 0 \tag{6}$$

of the radial equation (3a) becomes the familiar [25,26]

$$\frac{1}{2}\dot{r}^2 + V_{\text{eff}} = \varepsilon_{\text{eff}} \tag{7}$$

describing motion in the one-dimensional effective potential

$$V_{\text{eff}}(r, a = 0) \equiv -\frac{R(r)}{2r^4}\bigg|_{a=0} + \frac{1}{2}E^2$$

$$= -\frac{1}{r} + \frac{L_z^2}{2r^2} - \frac{L_z^2}{r^3} + \frac{1}{2}, \tag{8}$$

with effective energy $\varepsilon_{\text{eff}} = \frac{1}{2}E^2$. Note that the asymptotic value of the potential at $r = \infty$ is $1/2$, so that $E = 1$ divides bound from unbound motion.

An example of such an effective potential for a nonspinning black hole with $L_z = 3.55$ is shown in Fig. 2. It is simple to read from this figure that the maximum of the potential ($dV/dr = 0$, $d^2V/dr^2 < 0$) corresponds to an unstable circular orbit and the minimum of the potential ($dV/dr = 0$, $d^2V/dr^2 > 0$) corresponds to a stable circular orbit. Note that the energy of the maximum E_u is below the asymptotic value $E = 1$.

As indicated by the solid line, there is another orbit with energy E_u but an apastron given by the outer intersection of the horizontal line of energy E_u with V_{eff}. When released from rest at the apastron r_a, a test particle will roll toward the unstable circular orbit taking an infinite amount of time to reach the peak, and likewise if time reversed. This orbit is a homoclinic orbit. For every bound unstable circular
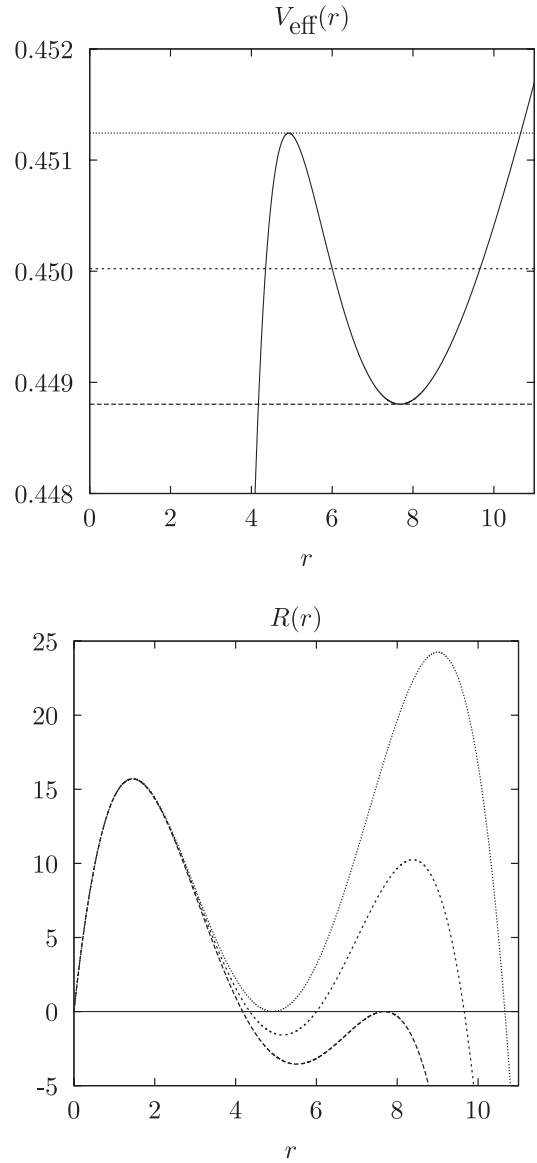

FIG. 2. $R(r)$ functions and $V_{\text{eff}}(r)$ (Eq. (8)) for 3 Schwarzschild orbits with $L_z = 3.55$. From bottom to top in both diagrams, the corresponding energies are $E = 0.947\,421$, $0.948\,707$, and $0.949\,993$. The first value is for a stable circular orbit at $r_s = 7.679\,020$, the second for an eccentric orbit with $r_p = 6.000\,593$ and $r_a = 9.656\,613$, and the third is for both an unstable circular orbit at $r_u = 4.923\,479$ and for a homoclinic orbit with $r_p = r_u$ and $r_a = 10.662\,889$. Note that $R(r) = R'(r) = 0$ at the circular orbits.

orbit there exists such a homoclinic orbit with the same E and L_z.[6] Appendix A shows that these are the only homoclinic orbits.

---

[6]There are no bound orbits with the same (E, L_z) of *unbound*, unstable circular orbits (i.e. those with $E > 1$) and therefore the unbound circular orbits do not possess homoclinic orbits, as elaborated in Appendix A.

For Kerr black holes ($a \neq 0$), the E and L_z dependences in Eq. (6) do not separate as they do in the Schwarzschild case. The radial motion can still be cast in the form (7) as the one-dimensional motion of a particle with energy

$$\varepsilon_{\text{eff}} = 0 \qquad (9a)$$

moving in a potential

$$V_{\text{eff}}(r) \equiv -R(r)/2\Sigma^2, \qquad (9b)$$

but unlike when $a = 0$, the potential depends on both E and L_z through $R(r)$. V_{eff} is thus a different potential for each orbit (i.e. for each (E, L_z) pair) instead of a single potential for an entire family of orbits like $V_{\text{eff}}(a = 0)$. Figure 2 plots various such functions $R(r)$ in the lower panel. As the figure highlights, having the potential vary under one's feet, so to speak, as the energy of the particle changes means that information we could previously glean from a single plot of $V_{\text{eff}}(a = 0)$ is now diluted over an infinite number of plots of $R(r)$.

Nevertheless, a bit more effort—expended in appendix A—shows that even when the black hole spins the unstable circular orbits are still the only hyperbolic invariant sets and that those with $E < 1$ give rise to homoclinic orbits. Finding the homoclinic orbits thus again amounts to finding the bound unstable circular orbits.

Plots of the $R(r)$ function can help us in this task. Although $R(r)$ changes with E, we can still read qualitative features of the motion effectively from a plot of $R(r)$. To clarify the visual interpretation, Fig. 2 plots $R(r)$ for $a = 0$, $L_z = 3.55$ and three different E values below a plot of the corresponding Schwarzschild $V_{\text{eff}}(r)$. Whereas in the effective potential diagram the r values accessible to a particle with given energy are those for which V_{eff} is below the constant energy line, in the pseudopotential diagram of a given orbit the accessible r values are those for which $R(r)$ is above the zero line, reflecting the fact that $\dot{r}$ in Eq. (3) is real so that the $R(r)$ under the radicand must be non-negative.

Turning points of the motion, for which $V_{\text{eff}}(r) = \varepsilon_{\text{eff}} = 0$, correspond to single roots of $R(r)$. Circular orbits require both $V_{\text{eff}} = 0$ and $dV_{\text{eff}}/dr = 0$, or the equivalent

$$R(r) = 0 \quad \text{and} \quad R'(r) = 0, \qquad (10)$$

and thus correspond to double roots of R, as Fig. 2 confirms. Simultaneously solving these equations yields expressions, originally published in Ref. [28],

$$E = \frac{r^{3/2} - 2r^{1/2} \pm a}{r^{3/4}\sqrt{r^{3/2} - 3r^{1/2} \pm 2a}} \qquad (11a)$$

$$L_z = \pm \frac{r^2 \mp 2ar^{1/2} + a^2}{r^{3/4}\sqrt{r^{3/2} - 3r^{1/2} \pm 2a}} \qquad (11b)$$

for the energy and angular momentum of circular orbits. The top/bottom signs denote prograde/retrograde.

Two noteworthy circular orbits demarcate the bound unstable ones: the innermost stable circular orbit (isco) and the innermost bound circular orbit (ibco). Figure 2 shows one unstable and one stable circular orbit for a single L_z. For any given a, this remains true for all $|L_z|$ above the minimum of (11b).[7] That minimum, for both $|L_z|$ and E, occurs at the isco [28]

$$r_{\text{isco}} = 3 + Z_2 \mp \sqrt{(3 - Z_1)(3 + Z_1 + 2Z_2)},$$

$$Z_1 \equiv 1 + \sqrt[3]{1 - a^2}[\sqrt[3]{1 + a^2} + \sqrt[3]{1 - a}], \qquad (12)$$

$$Z_2 \equiv \sqrt{3a^2 + Z_1^2},$$

where the stable and unstable circular orbits merge to a saddle point. Circular orbits with $r < r_{\text{isco}}$ are all unstable, with E and $|L_z|$ single valued and increasing as r decreases. E grows to 1 at the ibco [28]

$$r_{\text{ibco}} \equiv 2 \mp a + 2\sqrt{1 \mp a}. \qquad (13)$$

The upshot is that every $|L_{\text{isco}}| < |L_z| < |L_{\text{ibco}}|$ admits a bound unstable circular orbit and thus a corresponding homoclinic orbit with the same (E, L_z). The apastron of the homoclinic orbit with $(E_{\text{ibco}}, L_{\text{ibco}})$ is $r_a = \infty$ while the apastron (and periastron) of the homoclinic orbit with $(E_{\text{ibco}}, L_{\text{ibco}})$ is $r_a = r_{\text{isco}}$. In other words, the ibco has a homoclinic orbit with eccentricity 1 and the isco *is* a homoclinic orbit with eccentricity zero. The eccentricities of the homoclinic orbits range from 1 down to 0.

D. Exact expressions for orbital parameters of homoclinic orbits

Above we have described the homoclinic orbits by their E or L_z. There are other ways to describe the homoclinic orbits. In general, noncircular equatorial Kerr orbits form a two-parameter set, with any particular orbit specified by its energy and angular momentum. For bound nonplunging orbits, other pairs of independent orbital parameters can also be used, such as the periastron and apastron (r_p, r_a) or, as is often done, appropriately defined pseudo-Keplerian parameters (e, p) (eccentricity and semi-latus rectum, respectively). Homoclinic orbits, however, lie in one-to-one correspondence with the $E_u < 1$ unstable circular orbits, a one-parameter family specified by the radius r_u. Homoclinic orbits thus form a one-parameter family all of whose orbital parameters depend only on the single parameter r_u.

For E and L_z this is clearly the case—homoclinic orbits have the same energy and angular momentum as the circular orbit they asymptotically approach, and Eqs. (11) determine E and L_z once r_u is specified. Homoclinic orbits also form the separatrix between plunging and nonplung-

_____

[7]Statements that apply to both prograde and retrograde trajectories are phrased in terms of $|L_z|$

ing orbits, so they, like any bound nonplunging orbit, have well-defined values of r_p, r_a, e, p. Simple expressions for those parameters follow from rewriting the $R(r)$ function, which has a double root at r_u for homoclinic orbits, as

$$R(r) = (E^2 - 1)r(r - r_u)^2(r - r_a), \qquad (14)$$

where r_a is the apastron of the homoclinic orbit. Expanding (14) and equating powers of r with Eq. (5) for $R(r)$ yields relations among r_u, r_a, E and L_z. In particular, equality of the linear coefficients implies that

$$r_a = \frac{2(aE - L_z)^2}{(1 - E^2)r_u^2}. \qquad (15)$$

Substituting $E(r_u)$ and $L_z(r_u)$ from (11) for E and L_z and simplifying leads to the expression

$$r_a = \frac{2r_u(a \mp \sqrt{r_u})^2}{r_u^2 - 4r_u \pm 4a\sqrt{r_u} - a^2} \qquad (16)$$

for the apastron of a homoclinic orbit.

Equation (16) also furnishes expressions for the e and p of a homoclinic orbit in terms of r_u. As noted in [17] and references therein, Newtonian quantities like e and p have no unambiguous counterparts in general relativity. Nevertheless, even if their geometric meaning in the strong-field regime is debatable, the convention in the extreme mass ratio literature is to define the eccentricity and semi-latus rectum of a generic orbit by analogy with Keplerian orbits via

$$r_p \equiv \frac{p}{1 + e}, \qquad r_a \equiv \frac{p}{1 - e}, \qquad (17)$$

or equivalently

$$e \equiv \frac{r_a - r_p}{r_a + r_p} \qquad (18)$$

$$p \equiv \frac{2r_a r_p}{r_a + r_p}. \qquad (19)$$

We follow that convention here.[8]

Substituting (16) into (18) and (19) with $r_p = r_u$ yields

$$e^{\mathrm{hc}} = \frac{-r_u^2 + 6r_u \mp 8a\sqrt{r_u} + 3a^2}{r_u^2 - 2r_u + a^2} \qquad (20)$$

$$p^{\mathrm{hc}} = \frac{4r_u(a \mp \sqrt{r_u})^2}{r_u^2 - 2r_u + a^2}. \qquad (21)$$

---

[8]Note from (18) that, as with Keplerian orbits, e varies from 0 (for circular orbits, whose $r_a = r_p$) to 1 (for orbits with $E \to 1$, whose $r_a \to \infty$).

Reference [12] derives the implicit relation

$$0 = p^2(p - 6 - 2e)^2 + a^4(e - 3)^2(1 + e)^2$$
$$- 2a^2 p(1 + e)[14 + 2e^2 + p(3 - e)] \qquad (22)$$

that e and p of the homoclinic orbit (referred to there as "the separatix") must satisfy, and an equivalent implicit expression also appears in [1,13]. Acknowledging the relationship between the homoclinic orbits and unstable circular orbits from the outset furnishes the explicit parametric solutions (20) and (21) to those implicit equations.

We now know how to specify the equatorial circular orbits by a single parameter; either E or L_z for instance. The unstable circular orbits are a family of hyperolic sets, which means they have stable and unstable manifolds. We have also derived the perihelia and apastra of the homoclinic orbits as well as the (e, p) as explicit functions of r_u and spin.

However, we can do better than this. In the next section, we find exact solutions for the homoclinic trajectories themselves as a function of spin.

III. EXACT SOLUTIONS FOR EQUATORIAL HOMOCLINIC ORBITS

An exact solution to geodesic motion is a rare commodity. In this section we very briefly sketch the derivation of an exact parametric solution for homoclinic orbits around Kerr black holes of arbitrary spin and refer the reader to the acrobatics of Appendix A and B for the detailed derivation.

For any equatorial orbit, the radial motion consists of alternating inbound phases ($dr/d\tau < 0$) and outbound ($dr/d\tau > 0$) phases during which r varies monotonically with time. Because the equations of motion depend explicitly only on r, the radial coordinate parametrizes the motion during any single such phase, and other dynamical variables can be expressed in terms of r.

Consequently, during an inbound phase, the integrated proper time, coordinate time, and azimuth between some reference point r_0 and r are

$$\tau(r) = -\int_{r_0}^{r} dr \frac{d\tau}{dr} = -\int_{r_0}^{r} dr \frac{\Sigma}{\sqrt{R}} \qquad (23)$$

$$t(r) = -\int_{r_0}^{r} dr \frac{dt/d\tau}{dr/d\tau}$$
$$= -\int_{r_0}^{r} dr \frac{r^2(r^2 + a^2)E + 2a(aE - L_z)r}{\Delta\sqrt{R}} \qquad (24)$$

$$\varphi(r) = -\int_{r_0}^{r} dr \frac{d\varphi/d\tau}{dr/d\tau} = -\int_{r_0}^{r} dr \frac{r^2 L_z + 2(aE - L_z)r}{\Delta\sqrt{R}}, \qquad (25)$$

where r and r_0 are both radial coordinates along the same phase (i.e. along a given half-leaf) of the motion. Removing the overall minus signs yields the corresponding expressions for outbound motion. Equations (23)–(25) and their outbound counterparts are correct for both $r < r_0$ and $r > r_0$ along a single inbound/outbound phase.

For ordinary eccentric orbits, $R(r)$ has four distinct roots and Eqs. (23)–(25) are at best elliptic integrals. However, the fact that R factors as in (14) for homoclinic orbits renders the integrals soluble in terms of elementary functions. We integrate these equations analytically in appendix B to give:

$$\tau(r) = \frac{1}{\sqrt{1-E^2}}\sqrt{r(r_a - r)} + \frac{2}{(1-E^2)^{3/2}}\tan^{-1}\sqrt{\frac{r_a - r}{r}}$$
$$+ \frac{2}{\gamma\lambda_r}\tanh^{-1}\sqrt{\frac{r_u}{r_a - r_u}\frac{r_a - r}{r}} \tag{26a}$$

$$t(r) = \frac{E}{\sqrt{1-E^2}}\sqrt{r(r_a - r)} + 2E\frac{(3-2E^2)}{(1-E^2)^{3/2}}$$
$$\times \tan^{-1}\sqrt{\frac{r_a - r}{r}} + \frac{2}{\lambda_r}\tanh^{-1}\sqrt{\frac{r_u}{r_a - r_u}\frac{r_a - r}{r}}$$
$$- \frac{2r_+}{\sqrt{1-a^2}}\tanh^{-1}\sqrt{\frac{r_+}{r_a - r_+}\frac{r_a - r}{r}} - \frac{2r_-}{\sqrt{1-a^2}}$$
$$\times \tanh^{-1}\sqrt{\frac{r_-}{r_a - r_-}\frac{r_a - r}{r}} \tag{26b}$$

$$\varphi(r) = 2\frac{\Omega_u}{\lambda_r}\tanh^{-1}\sqrt{\frac{r_u}{r_a - r_u}\frac{r_a - r}{r}} - \frac{a}{\sqrt{1-a^2}}$$
$$\times \tanh^{-1}\sqrt{\frac{r_+}{r_a - r_+}\frac{r_a - r}{r}} - \frac{a}{\sqrt{1-a^2}}$$
$$\times \tanh^{-1}\sqrt{\frac{r_-}{r_a - r_-}\frac{r_a - r}{r}}, \tag{26c}$$

where we have set $\tau = t = \varphi = 0$ at $r = r_a$, the apastron (16) of the homoclinic orbit.

In the equations above, r_+ and r_- are, respectively, the (dimensionless) Boyer-Lindquist radial coordinates of the

outer and inner horizons of the black hole, $\gamma \equiv dt/d\tau(r_u)$ and $\Omega_u \equiv \frac{d\varphi}{dt}(r_u)$ are the (constant) Lorentz factor and azimuthal velocity ($\Omega_u > 0$ for prograde orbits, $\Omega_u < 0$ for retrograde) of the associated unstable circular orbit, and E is the energy of the homoclinic orbit (and also of the unstable circular orbit). The remaining parameter is

$$\lambda_r = \frac{1}{\gamma\Sigma}\sqrt{\frac{R''}{2}}\bigg|_{r_u}, \tag{27}$$

where a prime denotes differentiation with respect to r. (As derived in paper II in this series [16], λ_r is the radial stability exponent of the unstable circular orbit.)

Equation (26) reveals an interesting and unobvious fact about the homoclinic orbits. Consider a circular orbit at $r = r_u$ with energy E and L_z and a homoclinic orbit with the same energy and angular momentum. Even though the homoclinic orbit takes an infinite amount of time to asymptote to or away from r_u, the total accumulated phase difference between the homoclinic orbit and the circular orbit over that infinite period is finite.

To be concrete, consider a prograde homoclinic orbit with $t = 0$, $\varphi = 0$ at $r = r_a$, and let the circular orbit at r_u be at $\varphi = 0$ at the same time. Since r varies monotonically with t along the homoclinic orbit during its inbound phase (as $t \to \infty$), we can use the r coordinate along the homoclinic orbit as a global time parameter via Eq. (26b). Since φ along the circular orbit increases linearly at a rate $\omega_\varphi = \Omega_u$, the phase difference between the circular and homoclinic orbits is just the difference between

$$\varphi^{\text{circ}}(t(r)) = \Omega_u t(r), \tag{28}$$

and Eq. (26c). By time-reversal symmetry, doubling this yields the total phase difference between the circular and homoclinic orbits summed over both the inbound and outbound phases. Letting $t(r)$ denote time along the inbound ($\dot{r} < 0$) portion of the homoclinic orbit, the resulting phase difference

$$\Delta\varphi^{\text{hc}}(t(r)) \equiv 2[\varphi^{\text{circ}}(t(r)) - \varphi^{\text{hc}}(t(r))] = 2\Omega_u\frac{E}{\sqrt{1-E^2}}\left\{\sqrt{r(r_a - r)} + 2\frac{3-2E^2}{1-E^2}\tan^{-1}\sqrt{\frac{r_a - r}{r}}\right\}$$

$$= + \frac{2}{\sqrt{1-a^2}}\left\{(a - 2\Omega_u r_+)\tanh^{-1}\sqrt{\frac{r_+}{r_a - r_+}\frac{r_a - r}{r}} + (a - 2\Omega_u r_-)\tanh^{-1}\sqrt{\frac{r_-}{r_a - r_-}\frac{r_a - r}{r}}\right\} \tag{29}$$

diverges only for the homoclinic orbit with $r_u = r_{\text{ibco}}$ (for which $E = 1$, $r_a = \infty$). All other homoclinic orbits spend finite time at large distances from the circular orbit at r_u, and for them the limit

$$\lim_{t\to\infty}\Delta\varphi^{\text{hc}}(t) = \lim_{r\to r_u}\Delta\varphi^{\text{hc}}(r) \tag{30}$$
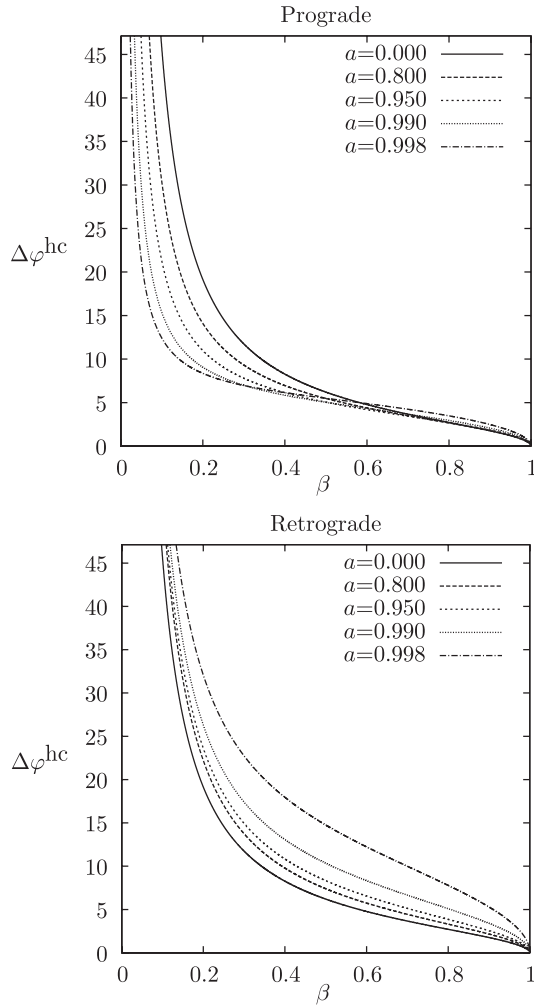
exists.

FIG. 3. The accumulated phase difference between a homoclinic orbit and the unstable circular orbit to which it is doubly asymptotic as a function of r_u. For a given spin a, the parameter β varies linearly from r_{ibco} when $\beta = 0$ to r_{isco} when $\beta = 1$. Upper: Prograde homoclinic orbits. Lower: Retrograde homoclinic orbits.

Figure 3 shows how $\Delta\varphi^{\mathrm{hc}}$ depends on r_u for various values of the black hole spin a. For ease of comparison, $\Delta\varphi^{\mathrm{hc}}$ is plotted versus a parameter that varies linearly from 0 when $r_u = r_{\mathrm{ibco}}$ to 1 when $r_u = r_{\mathrm{isco}}$ for a given a. The fact that $\Delta\varphi^{\mathrm{hc}} \bmod 2\pi \neq 0$ for all but a measure zero set of homoclinic orbits means that a generic equatorial homoclinic orbit asymptotes in the infinite future to a circular orbit out of phase by $\Delta\varphi^{\mathrm{hc}}$ with the circular orbit (at the same r_u) to which the homoclinic orbit asymptotes in the infinite past.[9]

---

[9]This is why we speak about an orbit being homoclinic to some invariant set (e.g., the locus of points in phase space with $r = r_u$, $p_r = 0$, φ arbitrary) and not about its being homoclinic to a particular *orbit* (e.g. a particular unstable circular orbit, including choice of phase).

Stated another way, if we were to treat all circular orbits at radius r_u with different phases as distinct, then by adding a constant and finite phase to any homoclinic orbit, we could speak meaningfully about synchronizing it with exactly one such circular orbit at $t = +\infty$ at r_u and with exactly one circular orbit at $t = -\infty$ also at r_u but with a different phase. Although a fine detail at this point, such phase information could be significant to gravitational wave templates for the full black hole spectrum.

IV. HOMOCLINIC LIMIT OF ZOOM-WHIRL ORBITS

Before concluding, we mention another perspective on the physical portrait of the homoclinic landmark, and that is the connection to zoom-whirl behavior. One visually striking feature of the homoclinic orbit of Fig. 1 is that it whirls an infinite number of times en route to the unstable circular orbit. This quintessential zoom-whirliness suggests an association between homoclinic orbits and non-homoclinic zoom-whirl orbits behavior that has long been suspected yet also subtly misunderstood. Many practitioners, including the present authors, suspected that zoom-whirl behavior was a consequence of proximity to the separatrix. It was also generally believed that zoom-whirliness was limited to orbits of moderate to high eccentricity.

To the contrary, we found in a previous work [11] that in the strong-field regime, Kerr test particle orbits *not* in the vicinity of the homoclinic orbit can also exhibit zoom-whirl behavior and that at least some zoom-whirl orbits exist for *any* eccentricity. Specifically, we reported that for low enough $|L_z|$ (strong-field regime), even vanishingly small perturbations to the stable circular orbit can whirl several times (in fact, an arbitrarily large number of times) per radial cycle.[10] Around black holes with spin parameter $a = 0$, by the time zoom-whirl orbits appear near the stable circular orbit, the effective potential is extremely shallow, with little difference between the energies of the stable circular and homoclinic orbits. Schwarzschild zoom-whirl orbits are thus still "close" to homoclinic orbits. As a increases, however, the depth of the potential at the $|L_z|$ at which low-eccentricity zoom-whirl orbits first appear increases. For high enough values of a, there are numerous orbits that whirl multiple times per radial cycle with eccentricities of $O(\sim 0.1)$ and that are not near the separatrix. Proximity to the separatrix, then, is a circumstantial and not intrinsic feature of zoom-whirl orbits.

---

[10]Admittedly, the whirl phases of these ultra-low eccentricity zoom-whirl orbits would be essentially indistinguishable from a circular orbit, both visually and in the variations of their emitted gravitational wave amplitude in the zoom versus whirl phases. Nevertheless, by the topological criteria of [11], they are *bona fide* zoom-whirl orbits.
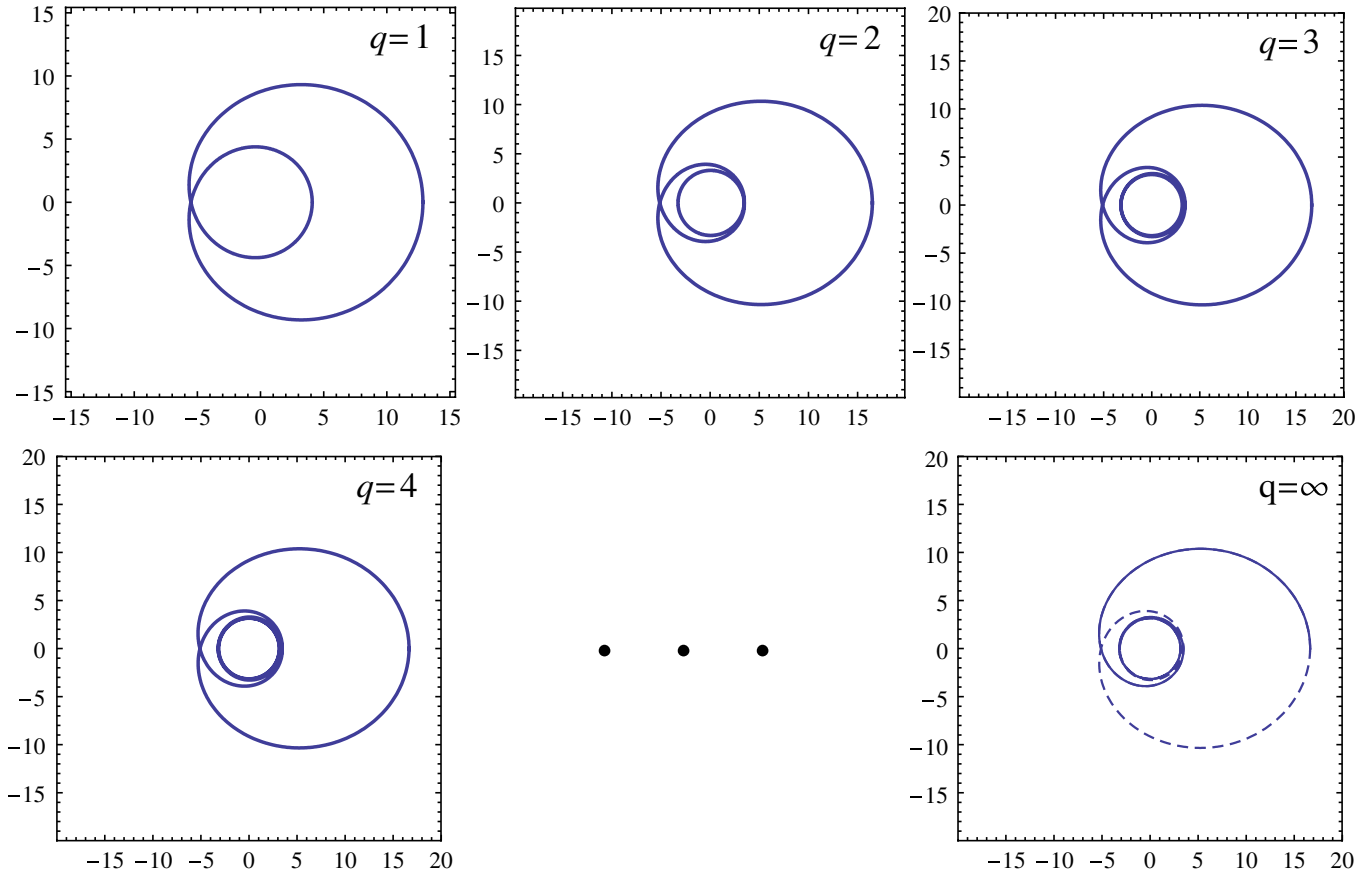
FIG. 4 (color online). The progression of the 1-leaf periodic orbits through $1, 2, 3, 4 \ldots \infty$ whirls. The orbits shown are prograde orbits for $a = 0.5$ and $L_z = 3.158\,540$, or the average of L_{isco} and L_{ibco}. Note that the whirls beyond the second whirl are too closely packed in r to distinguish visually in the plot.

Despite the fact that they are not responsible *per se* for zoom-whirl behavior, homoclinic orbits still have an important significance as the infinite whirl limit in the spectrum of zoom-whirl orbits, as we now make explicit. Reference [11] realized that the spectrum of all Kerr orbits naturally fall into periodic tables—tables with an infinite sequence of entries for a given orbital angular momentum, mass ratio and black hole spin.[11] Each entry in the periodic table is an exactly periodic orbit characterized by a rational number that immediately identifies the number of zooms, the number of whirls, and the order in which the zooms are executed.

The importance of the periodic tables lies in the observation that *every* bound orbit can be approximated to arbitrary precision by a periodic one. Perhaps more important to future studies of the dynamics, *every* bound orbit can be modeled as a slow precession around some low-leaf

periodic orbit, just as Mercury's orbit can be modeled as a precession around an ellipse.

Although homoclinic orbits are formally aperiodic in the sense that they never return to their initial conditions, they nonetheless mimic periodic orbits; in particular, they are the infinite whirl limit in the periodic sequence—the final entry in the infinite periodic table [11].

To make this connection explicit, consider single-leaf Kerr orbits like those in Fig. 4. Single-leaf orbits are in one-to-one correspondence with the whole numbers; that is, the rational associated with each one-leaf orbit counts the integer number of whirls. The final entry in this infinite list is the orbit that executes an infinite number of whirls and therefore never actually reaches the end of its first radial cycle. That orbit is of course the homoclinic orbit.

More specifically, if we denote by w the (integer) number of whirls made by a member of a constant L_z set of one-leaf orbits, then the sequences of energies E_w, eccentricities e_w, apastra r_{aw}, periastra r_{pw}, actions J_{rw}, etc. converge in the $w \to \infty$ limit to the values for the homoclinic orbit with the same L_z (for a black hole of a given spin).

As already noted, for a given a and L_z, the Kerr homoclinic orbits form the separatrix in the phase space between

_____

[11]The organization of orbits into periodic tables is not unique to the test particle limit. References [14,15] extend the taxonomy to mass ratios of $O(1)$ in a 3PN order Post-Newtonian expansion and identify homoclinic orbits in the same expansion.

orbits that plunge and those that do not. As discussed in detail in [11,22,23], orbits that are bound in the phase space turn out to lie on surfaces homeomorphic to 2-dimensional tori (3-tori for generic nonequatorial orbits), and only these bound orbits have an associated set of fundamental frequencies in terms of which orbit functionals can be Fourier expanded [6]. The homoclinic orbit of a given L is also therefore the separatrix between the regions of phase space inhabited by these quasiperiodic orbits and those that are fully aperiodic. Since all quasiperiodic orbits can be approximated by the periodic set, the homoclinic orbit is the divide between the domain of influence of the periodic set with its correspondence to the rationals and aperiodic orbits that merge or escape.

V. CONCLUSIONS

Homoclinic orbits offer the kind of crucial signpost that demarcates physically distinct regions of the conservative and inspiral dynamics: bound from plunging, whirling from not-whirling, smooth from chaotic. They thereby define salient details of black hole dynamics and we have spent time in this article deriving an exact parameteric solution for homoclinic motion that we hope will prove of use to others in the field.

Physically, we have shown that homoclinic trajectories are an infinite whirl limit of the zoom-whirl orbits. Even remembering that zoom-whirl behavior is generic and not exotic in the strong-field [11], the homoclinic orbits themselves are a special and sparse subset. Nonetheless, *every* inspiraling orbit should transit through a homoclinic orbit (or the remnant of one once all nonlinear relativistic effects are included) on the transition to plunge. The isco, which is the exit to plunge for quasicircular inspiral, is itself a homoclinic orbit with eccentricity zero. The homoclinic family ranges in eccentricity from zero (the isco) all the way up to 1 (homoclinic to the ibco). *All* orbits, except those exceptionally well-approximated as quasicircular, should roll through some member of the homoclinic family on the transition to plunge.

ACKNOWLEDGMENTS

APPENDIX A: THE EFFECTIVE POTENTIAL

1. $a = 0$

Although the key features of the Schwarzschild geometry are recognizable at a glance to anyone familiar with an effective potential formulation, the Kerr case is less visu-
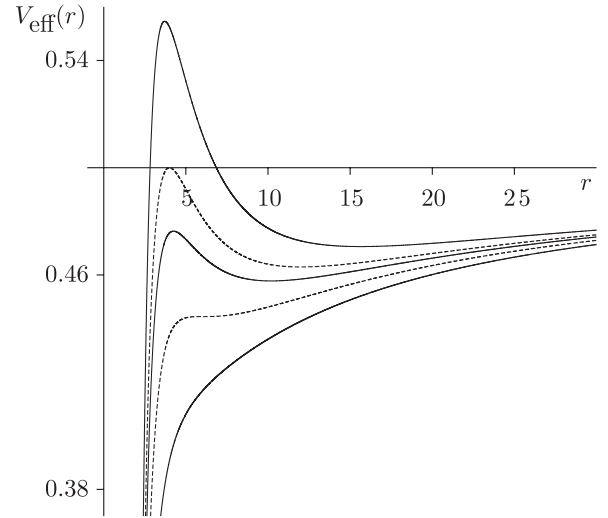

FIG. 5. The Schwarzschild effective potential drawn in solid lines as a function of radial coordinate r for $L_z = 3$, 3.8 and 4.4, from bottom to top. The upper and lower dashed lines represent the borderline potentials for $L_z = L_{ibco}$ and $L_z = L_{isco}$, respectively.

ally informative. In order to ground the details of the circular and homoclinic orbits, we include the Schwarzschild treatment in detail.

The value of L_z fixes the form of the potential, as shown in Fig. 5. Two critical values of L_z define regimes in which the potential exhibits different qualitative features: the angular momentum L_{isco} of the innermost stable circular orbit (isco), associated with the saddle point in the lower dashed potential, and the angular momentum L_{ibco} of the innermost bound circular orbit (ibco), the circular orbit with $E = 1$.

The effective potential picture allows us to determine the hyperbolic invariant sets at a glance:
  (1) No invariant set exists with $L_z < L_{isco}$, since every such orbit plunges and thus fails the recurrence test.
  (2) When $L_z > L_{isco}$, the potential admits one stable circular orbit with $r = r_s$, $E = E_s$ (minimum of $V_{eff}(a = 0)$) and one unstable circular orbit with $r = r_u$, $E = E_u$ (maximum of $V_{eff}(a = 0)$).
  (3) The value L_{ibco} further distinguishes the two subcases seen in Fig. 6, from which we see that orbits with $E \neq E_u$ never approach an invariant set. Instead, as $t \to \pm\infty$, every such orbit (a) oscillates between two turning points in the potential well, (b) plunges,[12] (c) escapes, or (d) escapes as $t \to -\infty$ and plunges as $t \to +\infty$ (or vice versa). None of the above asymptote to an invariant set.

---

[12]Equation (3d) implies that orbits plunge (reach the horizon) after a finite amount of proper time τ but an infinite amount of coordinate time t
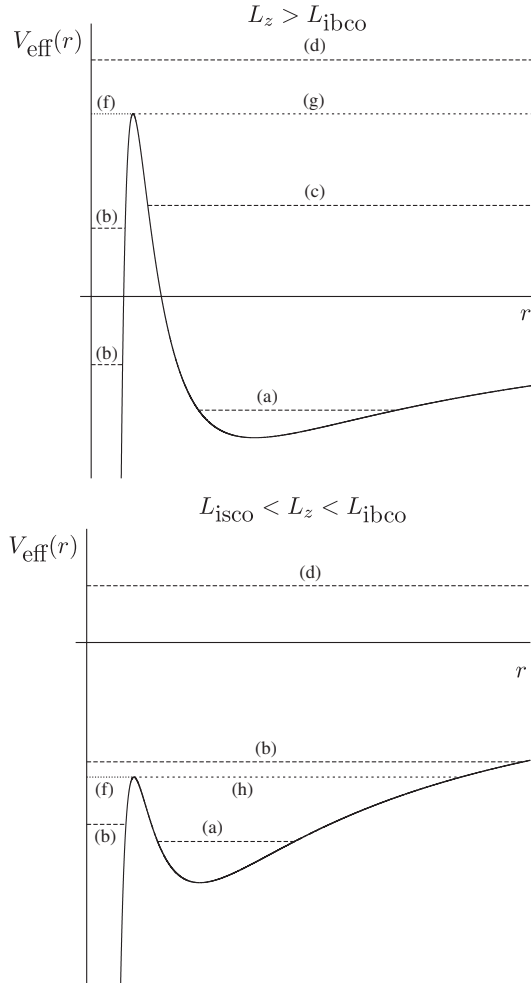
FIG. 6. Representative plots of the Schwarschild $V_{\text{eff}}(a = 0)$ for a value of $L_z > L_{\text{ibco}}$ (top) and $L_{\text{isco}} < L_z < L_{\text{ibco}}$ (bottom). As explained in the text, the horizontal lines define the energies ([for the fixed L_z of each $V_{\text{eff}}(a = 0)$] of orbits that (a) oscillate, (b) plunge, (c) escape to $r = \infty$, or (d) both plunge and access $r = \infty$, as $t \to \pm\infty$. The lines (f) and (g) tangent to $V_{\text{eff}}(a = 0)$ at $r = r_u$ represent $E = E_u$ orbits that asymptotically approach r_u at $t = +\infty$ or $-\infty$ [the ones marked (f) also plunge]. In the lower figure, the $E = E_u$ orbit (h) on the right also has a turning point, so it approaches r_u at both $t = \pm\infty$ and is homoclinic to the unstable circular orbit.

In contrast, orbits with $E = E_u$ do asymptotically approach an invariant set, namely, the unstable circular orbit. Consider the upper panel in Fig. 6, for which $L_z > L_{\text{ibco}}$. There is an $E = E_u$ orbit that approaches r_u as $t \to -\infty$ and plunges as $t \to +\infty$ and another that plunges as $t \to -\infty$ and approaches r_u as $t \to +\infty$, both represented by line (f) in the figure. These two orbits are distinct, just as the $E = E_u$ orbit that escapes as $t \to -\infty$ and approaches r_u as $t \to +\infty$ is distinct from its time-reversed counterpart [both represented by (g)]. So while they define stable and unstable manifolds for the circular orbit shown, these $E = E_u$ orbits are noninteresting [share no initial conditions $(r, \dot{r})$] and thus are not homoclinic to the circular orbit.

However, when $L_{\text{isco}} < L_z < L_{\text{ibco}}$, as in the lower panel of Fig. 5, the $E = E_u$ orbit (h) has a turning point and thus approaches r_u at both $t \to \pm\infty$. Parts of the stable and unstable manifolds of this unstable circular orbit intersect (in fact, they completely coincide), and these orbits are therefore homoclinic to the circular orbit.

We thus conclude that since they are the only recurrent orbits that are approached by any other orbit in the infinite future or past, the unstable circular orbits are the only hyperbolic invariant sets. Furthermore, those unstable circular orbits with $E < 1$ ($L_{\text{isco}} < L_z < L_{\text{ibco}}$) have associated homoclinic orbits with the same angular momentum and energy, or more specifically, a family of such orbits differing from one another by an overall translation in φ.

2. $a \neq 0$

Our argument will focus on the roots of the quartic R, which we can rewrite as

$$R(r) = (E^2 - 1)r(r - r_1)(r - r_2)(r - r_3). \qquad (A1)$$

For ease of notation, we adopt the conventions that, from left to right in (A1), real roots appear before complex roots and the nonzero real roots appear in ascending order $r_1 < r_2 < r_3$. Additionally,

$$R'(r = 0) > 0 \quad (\text{for } aE \neq L_z) \qquad (A2)$$

so R is negative just to the left and positive just to the right of the root at $r = 0$. Since complex roots occur in conjugate pairs, the zero root implies that at least one of the three remaining roots is real.

The non-negativity of $\dot{r}^2$ implies that motion is only possible where $R(r) \geq 0$. Turning points of the motion, for which $V_{\text{eff}}(r) = \varepsilon_{\text{eff}} = 0$, correspond to single roots of $R(r)$. Circular orbits require both $V_{\text{eff}} = 0$ and $dV_{\text{eff}}/dr = 0$, or the equivalent

$$R(r) = 0 \quad \text{and} \quad R'(r) = 0, \qquad (A3)$$

and thus correspond to double roots of R, as Fig. 2 confirms. Simultaneously solving these equations yields expressions [28]

$$E = \pm \frac{r^{3/2} - 2r^{1/2} \pm a}{r^{3/4}\sqrt{r^{3/2} - 3r^{1/2} \pm 2a}} \qquad (A4a)$$

$$L_z = \pm \frac{r^2 \mp 2ar^{1/2} + a^2}{r^{3/4}\sqrt{r^{3/2} - 3r^{1/2} \pm 2a}} \qquad (A4b)$$

for the energy and angular momentum of circular orbits, where the top/bottom signs apply to prograde/retrograde orbits. These functions, plotted for a sample of a values in Fig. 7 simultaneous minima (maxima for retrograde L_z) at [28]
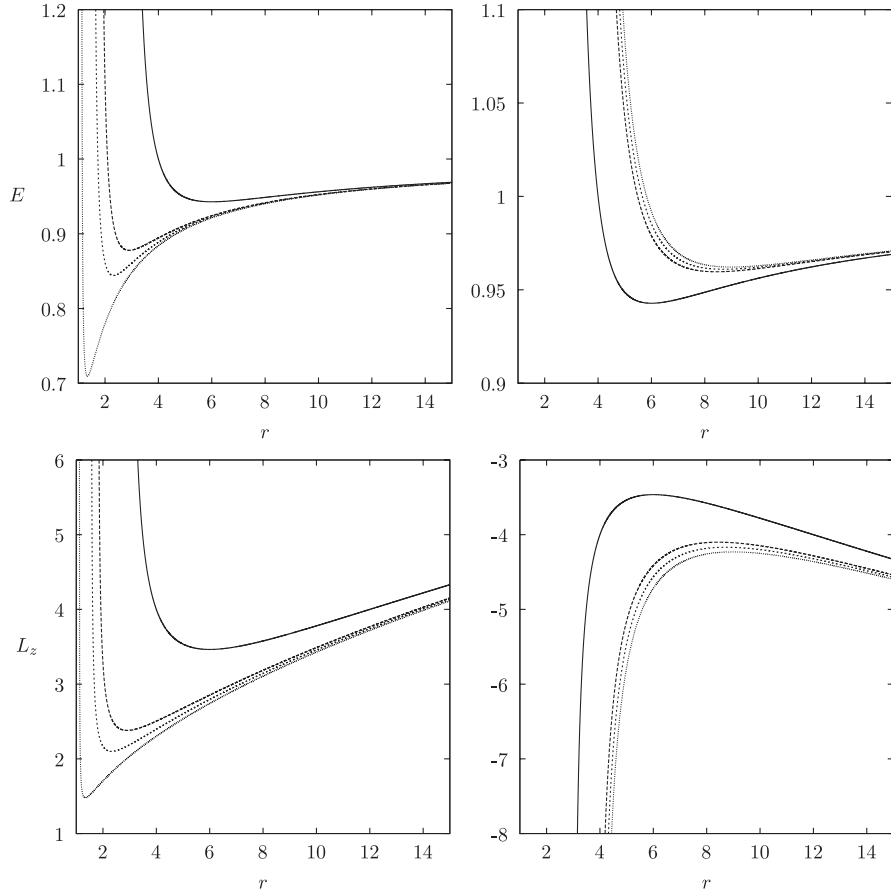
FIG. 7. E and L_z as functions of the radius r of prograde (left panels) and retrograde (right panels) circular orbits. The spin parameter for the curves are $a = 0$ (solid curve), and then in order of increasing distance from the solid curves, $a = 0.8$, 0.9, and 0.995. For a given a, E and L_z have simultaneous minima at $r = r_{\text{isco}}$.

$$r_{\text{isco}} = 3 + Z_2 \mp \sqrt{(3 - Z_1)(3 + Z_1 + 2Z_2)},$$

$$Z_1 \equiv 1 + \sqrt[3]{1 - a^2}[\sqrt[3]{1 + a} + \sqrt[3]{1 - a}], \qquad (\text{A5})$$

$$Z_2 \equiv \sqrt{3a^2 + Z_1^2}.$$

We note that the only solution to $R''(r) = 0$ consistent with (A4) occurs when $r = r_{\text{isco}}$, $E = E_{\text{isco}}$, $|L_z| = |L_{\text{isco}}|$. Thus, the isco corresponds to the only possible triple root of R (since a triple root of a function requires that the function and its first two derivatives vanish).

Furthermore, since

$$\left.\frac{\partial^2 V_{\text{eff}}}{\partial r^2}\right|_{R=0,R'=0} = -\frac{R''(r)}{2\Sigma^2}, \qquad (\text{A6})$$

R'' also determines the stability of circular orbits, with 1

$$\begin{aligned} r < r_{\text{isco}} &\Rightarrow R''(r) > 0 \Rightarrow \text{unstable} \\ r > r_{\text{isco}} &\Rightarrow R''(r) < 0 \Rightarrow \text{stable} \end{aligned} \qquad (\text{A7})$$

for a given $|L_z| > |L_{\text{isco}}|$. Also, paralleling the $a = 0$ case, $E(r)$ in (A4a) increases monotonically for $r > r_{\text{isco}}$ and approaches 1 as $r \to \infty$, so that stable circular orbits al-

ways have $E_{\text{isco}} < E < 1$. Unstable circular orbits, on the other hand, can have any $E > E_{\text{isco}}$, and the circular orbit with $E = 1$ occurs at [28]

$$r_{\text{ibco}} \equiv 2 \mp a + 2\sqrt{1 \mp a}. \qquad (\text{A8})$$

We now show that every noncircular Kerr equatorial orbit falls into one of the same categories listed for Schwarzschild orbits in Fig. 6. Recall that each $R(r)$ plot represents only those orbits with the same E and L_z and that motion is only possible in regions where $R > 0$. When $E > 1$, $R(r) \to +\infty$ at both $r \to \pm\infty$, and (A2) implies that R has a negative root. There are thus three possibilities for the number and type of positive roots:

(1) No positive roots, in which case all positive r are accessible, and R represents a single type (d) orbit.

(2) Two positive roots $r_2 < r_3$, resulting in a type (b) orbit ($0 \leq r \leq r_2$) and a type (c) orbit ($r \geq r_3$).

(3) One positive double root $r_2 = r_3 \equiv r_u$ with $R''(r_u) > 0$, in which case R represents an $E_u > 1$ circular orbit at $r = r_u$ plus orbits of type (f) ($0 \leq r \leq r_u$) and (g) ($r \geq r_u$) that asymptotically ap-

proach r_u in either the infinite future or past (but not both).

The $E = 1$ case is the same as above but without the negative root (since R is only cubic when $E = 1$). We thus conclude as in the $a = 0$ case that the invariant sets with $E \geq 1$ are unstable circular orbits but that they do not have orbits homoclinic to them.

When $E < 1$, $R \to \infty$ at $r \to \pm\infty$. Equation (A2) requires that there be at least one positive root and only an even number of negative roots, leaving four possibilities for the number and type of positive roots:

(1) Just the one root r_1, resulting in a type (b) orbit ($0 \leq r \leq r_1$)

(2) Three total positive roots $r_1 < r_2 < r_3$, resulting in a type (b) orbit ($0 \leq r \leq r_1$) and an oscillatory bound orbit of type (a) ($r_2 \equiv r_p \leq r \leq r_3 \equiv r_a$).

(3) One single positive root r_1 and one double root $r_2 \equiv r_s > r_1$ with $R''(r_s) < 0$, denoting a type (b) orbit ($0 \leq r \leq r_1$) and a stable circular orbit of radius r_s.

(4) One single root r_2 and one double root at $r_1 \equiv r_u < r_2$ with $R''(r_u) > 0$, so that $R(r)$ features an unstable circular orbit with $E_u < 1$ at r_u, a type (b) orbit ($0 \leq r \leq r_1$), and a type (h) orbit ($r_u \leq r \leq r_2 \equiv r_a$) that approaches r_u as $t \to \pm\infty$, i.e. an orbit homoclinic to r_u.

As before, we conclude that the invariant sets with homoclinic orbits are the unstable circular orbits with $E_u < 1$, one of which exists for every $r_{\text{ibco}} < r_u < r_{\text{isco}}$.

APPENDIX B: DERIVATION OF EQUATORIAL HOMOCLINIC ORBITS

We now find an exact solution by analytically integrating the following equations:

$$\tau(r) = -\int_{r_0}^{r} dr \frac{d\tau}{dr} = -\int_{r_0}^{r} dr \frac{\Sigma}{\sqrt{R}}, \qquad (B1)$$

$$t(r) = -\int_{r_0}^{r} dr \frac{dt/d\tau}{dr/d\tau}$$
$$= -\int_{r_0}^{r} dr \frac{r^2(r^2 + a^2)E + 2a(aE - L_z)r}{\Delta\sqrt{R}}, \qquad (B2)$$

$$\varphi(r) = -\int_{r_0}^{r} dr \frac{d\varphi/d\tau}{dr/d\tau} = -\int_{r_0}^{r} dr \frac{r^2L + 2(aE - L_z)r}{\Delta\sqrt{R}}, \qquad (B3)$$

where r and r_0 are both radial coordinates along the same phase (i.e. along a given half-leaf) of the motion. Removing the overall minus signs yields the corresponding expressions for outbound motion.

1. Integral equations for homoclinic orbits

Some algebraic manipulation of the denominators of the integrals (B1)–(B3) renders them more suitable for evaluation. We begin with $R(r)$, which for equatorial orbits has its smallest root at $r = 0$ (since $Q = 0$). For homoclinic orbits specifically, the remaining roots of R are a double root at $r_u(= r_p)$ and a simple root at r_a. $R(r)$ therefore factors into

$$R(r) = (E^2 - 1)(r - r_u)^2 r(r - r_a) \qquad (B4)$$

$$= (1 - E^2)(r - r_u)^2 r(r_a - r), \qquad (B5)$$

where we have written R in the second form so that the product of the r-dependent terms is manifestly positive for $r_p < r < r_a$. The square root in the denominators thus becomes

$$\sqrt{R(r)} = \sqrt{1 - E^2}(r - r_u)\sqrt{r(r_a - r)}, \qquad (B6)$$

where we have replaced $\sqrt{(r - r_u)^2}$ with $(r - r_u)$ since $r > r_u$ over the entire orbit. Δ also factors into

$$\Delta = (r - r_+)(r - r_-), \qquad (B7)$$

where $r_+ \equiv 1 + \sqrt{1 - a^2}$ and $r_- \equiv 1 - \sqrt{1 - a^2}$ are the outer and inner horizons, respectively, of the central black hole. The integrals (B1)–(B3) are therefore

$$\tau(r) = -\frac{1}{\sqrt{1 - E^2}} \int_{r_0}^{r} dr \frac{r^2}{(r - r_u)\sqrt{r(r_a - r)}}, \qquad (B8)$$

$$t(r) = -\frac{1}{\sqrt{1 - E^2}}$$
$$= \int_{r_0}^{r} dr \frac{r^2(r^2 + a^2)E + 2a(aE - L_z)r}{(r - r_+)(r - r_-)(r - r_u)\sqrt{r(r_a - r)}}, \qquad (B9)$$

$$\varphi(r) = -\frac{1}{\sqrt{1 - E^2}}$$
$$= \int_{r_0}^{r} dr \frac{r^2L_z + 2(aE - L_z)r}{(r - r_+)(r - r_-)(r - r_u)\sqrt{r(r_a - r)}}. \qquad (B10)$$

2. Change of variable

We can express the integrals above more compactly as

$$\tau(r) = \frac{1}{\sqrt{1 - E^2}} I_1 \qquad (B11)$$

$$t(r) = \frac{1}{\sqrt{1 - E^2}} \times [EI_2 + a^2EI_3 + 2a(aE - L_z)I_4], \qquad (B12)$$

$$\varphi(r) = \frac{1}{\sqrt{1 - E^2}}[L_z I_3 + 2(aE - L_z)I_4], \quad \text{(B13)}$$

where

$$I_1 \equiv -\int_{r_0}^{r} dr \frac{r^2}{(r - r_u)\sqrt{r(r_a - r)}}, \quad \text{(B14a)}$$

$$I_2 \equiv -\int_{r_0}^{r} dr \frac{r^4}{(r - r_+)(r - r_-)(r - r_u)\sqrt{r(r_a - r)}}, \quad \text{(B14b)}$$

$$I_3 \equiv -\int_{r_0}^{r} dr \frac{r^2}{(r - r_+)(r - r_-)(r - r_u)\sqrt{r(r_a - r)}}, \quad \text{(B14c)}$$

$$I_4 \equiv -\int_{r_0}^{r} dr \frac{r}{(r - r_+)(r - r_-)(r - r_u)\sqrt{r(r_a - r)}}, \quad \text{(B14d)}$$

We evaluate each of the integrals in (B14) in closed form by the same procedure. First, we bring one (positive definite) r from each numerator under a radical as an r^2:

$$I_1 = -\int_{r_0}^{r} dr \sqrt{\frac{r}{r_a - r}} \frac{r}{(r - r_u)}, \quad \text{(B15a)}$$

$$I_2 = -\int_{r_0}^{r} dr \sqrt{\frac{r}{r_a - r}} \frac{r^3}{(r - r_+)(r - r_-)(r - r_u)}, \quad \text{(B15b)}$$

$$I_3 = -\int_{r_0}^{r} dr \sqrt{\frac{r}{r_a - r}} \frac{r}{(r - r_+)(r - r_-)(r - r_u)}, \quad \text{(B15c)}$$

$$I_4 = -\int_{r_0}^{r} dr \sqrt{\frac{r}{r_a - r}} \frac{1}{(r - r_+)(r - r_-)(r - r_u)}. \quad \text{(B15d)}$$

Next, the change of variable

$$u = \sqrt{\frac{r_a - r}{r}}, \qquad r = \frac{r_a}{u^2 + 1},$$

$$-dr \sqrt{\frac{r}{r_a - r}} = du \frac{2r_a}{(u^2 + 1)^2} \quad \text{(B16)}$$

turns the integrals (B15) into

$$I_1 = 2r_a^2 \int_{u_0}^{u} du \frac{1}{y^2(r_a - r_u y)}, \quad \text{(B17a)}$$

$$I_2 = 2r_a^4 \int_{u_0}^{u} du \frac{1}{y^2(r_a - r_+ y)(r_a - r_- y)(r_a - r_u y)}, \quad \text{(B17b)}$$

$$I_3 = 2r_a^2 \int_{u_0}^{u} du \frac{1}{(r_a - r_+ y)(r_a - r_- y)(r_a - r_u y)}, \quad \text{(B17c)}$$

$$I_4 = 2r_a \int_{u_0}^{u} du \frac{y}{(r_a - r_+ y)(r_a - r_- y)(r_a - r_u y)}, \quad \text{(B17d)}$$

where we have written $y \equiv u^2 + 1$ as a shorthand.

3. Partial fraction decomposition

Each integrand in (B17) is now a product of factors linear in y and splits up via a standard partial fraction decomposition. We get

$$I_1 = 2\int_{u_0}^{u} du \left[\frac{A_{11}}{y^2} + \frac{A_{12}}{y} + \frac{A_{13}}{r_a - r_u y}\right], \quad \text{(B18a)}$$

$$I_2 = 2\int_{u_0}^{u} du \left[\frac{A_{21}}{y^2} + \frac{A_{22}}{y} + \frac{A_{23}}{r_a - r_u y} + \frac{A_{24}}{r_a - r_+ y} + \frac{A_{25}}{r_a - r_- y}\right], \quad \text{(B18b)}$$

$$I_3 = 2\int_{u_0}^{u} du \left[\frac{A_{33}}{r_a - r_u y} + \frac{A_{34}}{r_a - r_+ y} + \frac{A_{35}}{r_a - r_- y}\right], \quad \text{(B18c)}$$

$$I_4 = 2\int_{u_0}^{u} du \left[\frac{A_{43}}{r_a - r_u y} + \frac{A_{44}}{r_a - r_+ y} + \frac{A_{45}}{r_a - r_- y}\right], \quad \text{(B18d)}$$

where

$$A_{11} = r_a = A_{21}, \qquad A_{12} = r_u,$$

$$A_{22} = r_u + r_+ + r_-, \qquad A_{13} = r_u^2, \qquad A_{23} = r_u^3 A_{43},$$

$$A_{33} = r_u A_{43}, \qquad A_{43} = \frac{r_u}{(r_u - r_+)(r_u - r_-)},$$

$$A_{24} = r_+^3 A_{44}, \qquad A_{34} = r_+ A_{44},$$

$$A_{44} = \frac{-r_+}{(r_+ - r_-)(r_u - r_+)}, \qquad A_{25} = r_-^3 A_{45},$$

$$A_{35} = r_- A_{45}, \qquad A_{45} = \frac{r_-}{(r_+ - r_-)(r_u - r_-)}. \quad \text{(B19)}$$

We are left with five different integrals to calculate. Recalling that $y = u^2 + 1$, those antiderivatives evaluate to

$$\mathcal{I}_1 \equiv \int du \frac{1}{y^2} = \int du \frac{1}{(u^2 + 1)^2} = \frac{1}{2}\left(\frac{u}{1 + u^2} + \tan^{-1}u\right), \quad \text{(B20a)}$$

$$\mathcal{I}_2 \equiv \int du \frac{1}{y} = \int du \frac{1}{u^2 + 1} = \tan^{-1}u, \quad \text{(B20b)}$$

$$\mathcal{I}_3 \equiv \int du \frac{1}{r_a - r_u y} = \int du \frac{1}{(r_a - r_u) - r_u u^2}$$
$$= \frac{1}{\sqrt{r_u}\sqrt{r_a - r_u}}\tanh^{-1}\left\{u\sqrt{\frac{r_u}{r_a - r_u}}\right\}, \quad \text{(B20c)}$$

$$\mathcal{I}_4 \equiv \int du \frac{1}{r_a - r_+ y} = \int du \frac{1}{(r_a - r_+) - r_+ u^2}$$
$$= \frac{1}{\sqrt{r_+}\sqrt{r_a - r_+}}\tanh^{-1}\left\{u\sqrt{\frac{r_+}{r_a - r_+}}\right\}, \quad \text{(B20d)}$$

$$\mathcal{I}_5 \equiv \int du \frac{1}{r_a - r_- y} = \int du \frac{1}{(r_a - r_-) - r_- u^2}$$
$$= \frac{1}{\sqrt{r_-}\sqrt{r_a - r_-}}\tanh^{-1}\left\{u\sqrt{\frac{r_-}{r_a - r_-}}\right\}. \quad \text{(B20e)}$$

The integrals (B18) are therefore

$$I_1 = 2(A_{11}\mathcal{I}_1 + A_{12}\mathcal{I}_2 + A_{13}\mathcal{I}_3), \tag{B21a}$$

$$I_2 = 2(A_{21}\mathcal{I}_1 + A_{22}\mathcal{I}_2 + A_{23}\mathcal{I}_3 + A_{24}\mathcal{I}_4 + A_{25}\mathcal{I}_5), \tag{B21b}$$

$$I_3 = 2(A_{33}\mathcal{I}_3 + A_{34}\mathcal{I}_4 + A_{35}\mathcal{I}_5), \tag{B21c}$$

$$I_4 = 2(A_{43}\mathcal{I}_3 + A_{44}\mathcal{I}_4 + A_{45}\mathcal{I}_5). \tag{B21d}$$

Combining Eqs. (B11)–(B13) and (B19)–(B21), and recalling that $u = \sqrt{(r_a - r)/r}$, the dynamical variables τ, t and φ become

$$\tau(r) = \frac{1}{\sqrt{1 - E^2}} \sum_{j=1}^{3} C_j^{(\tau)} f_j(r), \tag{B22}$$

$$t(r) = \frac{1}{\sqrt{1 - E^2}} \sum_{j=1}^{5} C_j^{(t)} f_j(r), \tag{B23}$$

$$\varphi(r) = \frac{1}{\sqrt{1 - E^2}} \sum_{j=3}^{5} C_j^{(\varphi)} f_j(r), \tag{B24}$$

where the functions $f_j(r)$ are

$$f_1(r) = \sqrt{r(r_a - r)}, \tag{B25a}$$

$$f_2(r) = \tan^{-1}\sqrt{\frac{r_a - r}{r}}, \tag{B25b}$$

$$f_3(r) = \tanh^{-1}\sqrt{\frac{r_u}{r_a - r_u}\frac{r_a - r}{r}}, \tag{B25c}$$

$$f_4(r) = \tanh^{-1}\sqrt{\frac{r_+}{r_a - r_+}\frac{r_a - r}{r}}, \tag{B25d}$$

$$f_5(r) = \tanh^{-1}\sqrt{\frac{r_-}{r_a - r_-}\frac{r_a - r}{r}}, \tag{B25e}$$

and the corresponding coefficients are

$$C_1^{(\tau)} = 1, \qquad C_2^{(\tau)} = (r_a + 2r_u), \qquad C_3^{(\tau)} = 2\sqrt{\frac{r_u^3}{r_a - r_u}}, \qquad C_1^{(t)} = E, \qquad C_2^{(t)} = E(r_a + 2(r_u + 2)),$$

$$C_3^{(t)} = 2\sqrt{\frac{r_u^3}{r_a - r_u}}\frac{r_u^2(r_u^2 + a^2)E + 2a(aE - L_z)r_u}{(r_u - r_+)(r_u - r_-)r_u^2}, \qquad C_3^{(\varphi)} = 2\sqrt{\frac{r_u^3}{r_a - r_u}}\frac{r_u^2 L_z + 2(aE - L_z)r_u}{(r_u - r_+)(r_u - r_-)r_u^2},$$

$$C_4^{(t)} = \frac{-4r_+}{r_+ - r_-}\frac{2Er_+ - aL_z}{\sqrt{r_+(r_a - r_+)(r_u - r_+)}}, \qquad C_4^{(\varphi)} = \frac{-2r_+}{r_+ - r_-}\frac{2aE - L_z r_-}{\sqrt{r_+(r_a - r_+)(r_u - r_+)}}, \tag{B26}$$

$$C_5^{(t)} = \frac{4r_-}{r_+ - r_-}\frac{2Er_- - aL_z}{\sqrt{r_-(r_a - r_-)(r_u - r_-)}}, \qquad C_5^{(\varphi)} = \frac{2r_-}{r_+ - r_-}\frac{2aE - L_z r_+}{\sqrt{r_-(r_a - r_-)(r_u - r_-)}}.$$

In the expressions above, we have used the facts that (since $r_\pm$ are roots of Δ) $r_\pm^2 + a^2 = 2r_\pm$ and that $r_+ + r_- = 2$. Note that since all of the $f_j(r)$ vanish at $r = r_a$, our expressions (B22)–(B24) implicitly assume the natural choice of time and azimuthal origins, namely, at apastron. After all, since they are single-leaf orbits with formally infinite radial periods, homoclinic orbits have only 1 outbound and 1 inbound phase each and transit through apastron only once. We now make that choice explicit. From here on, all expressions assume that

$$\tau(r_a) = t(r_a) = \varphi(r_a) = 0, \tag{B27}$$

along homoclinic orbits, so that τ and t are positive/negative along the inbound/outbound branch, while φ is positive/negative along the inbound/outbound branch for prograde orbits (increasing φ) and negative/positive along the inbound/outbound branch for retrograde orbits (decreasing φ).

4. Simplification of coefficients

The task now is to render the coefficients in a more meaningful form. The C_1's are already simple. To simplify the C_2's, we expand the factored form (B5) of $R(r)$ to

$$R(r) = (1 - E^2)\{-r^4 + (2r_u + r_a)r^3 - r_u(2r_a + r_u)r^2 + r_u^2 r_a r\}. \tag{B28}$$

Comparing to (5) (with $Q = 0$) and equating coefficients of corresponding powers of r, we see that for equatorial homoclinic orbits,

$$r_a + 2r_u = \frac{2}{1 - E^2}. \tag{B29}$$

Thus, the C_2's are

$$C_2^{(\tau)} = \frac{2}{1 - E^2}, \tag{B30}$$

$$C_2^{(t)} = E\left(\frac{2}{1 - E^2} + 4\right) = 2E\left(\frac{3 - 2E^2}{1 - E^2}\right). \tag{B31}$$

For the C_3's, notice that

$$R''(r) = (1 - E^2)\{-12r^2 + 6(2r_u + r_a)r - 2r_u(2r_a + r_u)\} \tag{B32}$$

$$\Rightarrow R''(r_u) = (1 - E_u^2)2r_u(r_a - r_u) \tag{B33}$$

Inserting this into the expression for the proper time stability exponent $\gamma \lambda_r$ of the unstable circular orbit associated with the homoclinic orbit yields

$$\gamma \lambda_r = \sqrt{\frac{R''(r_u)}{2\Sigma_u^2}} = \sqrt{1 - E_u^2}\sqrt{\frac{2r_u(r_a - r_u)}{2r_u^4}}$$

$$= \sqrt{1 - E_u^2}\sqrt{\frac{r_a - r_u}{r_u^3}}. \qquad (B34)$$

The coefficient $C_3^{(\tau)}$ is therefore

$$C_3^{(\tau)} = 2\sqrt{\frac{r_u^3}{r_a - r_u}} = \frac{2}{\gamma \lambda_r}\sqrt{1 - E_u^2}. \qquad (B35)$$

$C_3^{(t)}$ and $C_3^{(\varphi)}$ are each $C_3^{(\tau)}$ times another factor. Comparing to (B1) and (B3), however, we can identify these extra factors as the $dt/d\tau$ and $d\varphi/d\tau$, respectively, of the unstable circular orbit associated with the homoclinic orbit. That allows us to write

$$C_3^{(t)} = \frac{2}{\gamma \lambda_r}\sqrt{1 - E^2}\frac{dt}{d\tau}(r_u) = \frac{2}{\lambda_r}\sqrt{1 - E^2}, \qquad (B36)$$

where λ_r, as we will show in paper II [16], refers to the stability exponent governing the evolution with respect to coordinate time t of small perturbations to the circular orbit (we have used here the fact that $\lambda_r dt = \gamma \lambda_r d\tau$). Likewise,

$$C_3^{(\varphi)} = \frac{2}{\gamma \lambda_r}\sqrt{1 - E^2}\frac{d\varphi}{d\tau}(r_u) = \frac{2}{\lambda_r}\frac{d\tau}{dt}(r_u)\frac{d\varphi}{d\tau}(r_u)$$

$$= \frac{2}{\lambda_r}\sqrt{1 - E^2}\frac{d\varphi}{d\tau}(r_u) = 2\frac{\Omega_u}{\lambda_r}\sqrt{1 - E^2}, \qquad (B37)$$

where $\Omega_u \equiv \frac{d\varphi}{dt}(r_u)$.

Simplifying the C_4's takes a little more work. As mentioned in Sec. II, the energy and angular momentum of the homoclinic orbit are the same as those of the unstable circular orbit at r_u. Recalling the expressions (A4b) for circular orbits (top/bottom signs are for prograde/retrograde orbits) from [28], we can rewrite the numerator of the second factor in $C_4^{(t)}$ as

$$2Er_+ - aL_z = \frac{(2r + r_u^{3/2} - 2r_u^{1/2} \pm a) \mp a(r_u^2 \mp 2ar_u^{1/2} + a^2)}{r_u^{3/4}\sqrt{r_u^{3/2} - 3r_u^{1/2} \pm 2a}} = \frac{[2r_+ r_u^{3/2} - 4r_+ r_u^{1/2} + 2\underbrace{\overset{2}{a} r_u^{1/2}}_{r_+ r_-}] \mp a[r_u^2 \underbrace{-2r_+ + a^2}_{-r_+^2}]}{r_u^{3/4}\sqrt{r_u^{3/4} - 3r_u^{1/2} \pm 2a}}$$

$$= \frac{2r_+ r_u^{1/2}(r_u \underbrace{-2 + r_-}_{-r_+}) \mp a(r_u - r_+)(r_u + r_+)}{r_u^{3/4}\sqrt{r_u^{3/2} - 3r_u^{1/2} \pm 2a}} = \frac{(r_u - r_+)[2r_+ r_u^{1/2} \mp a(r_u + r_+)]}{r_u^{3/4}\sqrt{r_u^{3/2} - 3r_u^{1/2} \pm 2a}} \qquad (B38)$$

where we have used the facts that $r_\pm$ are roots of Δ and that $r_+ r_- = a^2$. Analogously, the numerator of the second factor in $C_5^{(t)}$ becomes

$$2Er_- - aL_z = \frac{(r_u - r_-)[2r_- r_u^{1/2} \mp a(r_u + r_-)}{r_u^{3/4}\sqrt{r_u^{3/2} - 3r_u^{1/2} \pm 2a}}, \qquad (B39)$$

leaving the coefficients $C_{4,5}^{(t)}$ as

$$C_4^{(t)} = \frac{-4r_+}{r_+ - r_-}\frac{1}{\sqrt{r_u^{3/2}(r_u^{3/2} - 3r_u^{1/2} \pm 2a}}$$

$$\times \frac{2r_+ r_u^{1/2} \mp a(r_u + r_+)}{\sqrt{r_+(r_a - r_+)}}, \qquad (B40)$$

$$C_5^{(t)} = \frac{4r_-}{r_+ - r_-}\frac{1}{\sqrt{r_u^{3/2}(r_u^{3/2} - 3r_u^{1/2} \pm 2a)}}$$

$$\times \frac{2r_- r_u^{1/2} \mp a(r_u + r_-)}{\sqrt{r_-(r_a - r_-)}}. \qquad (B41)$$

For what follows, it will be useful to look at the signs of the numerators

$$2r_+ r_u^{1/2} \mp a(r_u + r_+), \quad \text{for } C_4 \qquad (B42)$$

$$2r_- r_u^{1/2} \mp a(r_u + r_-), \quad \text{for } C_5. \qquad (B43)$$

In the retrograde case (bottom sign), each is the sum of two non-negative terms and thus strictly non-negative. In the prograde case (top sign), we can whether the sign depends on the values of r_u and a by treating each of (B42) and (B43) as quadratic function of the variable $y = r_u^{1/2}$. Specifically, those functions will be *negative* when

$$ay^2 - 2r_+ y + ar_+ > 0, \quad \text{for } C_4 \qquad (B44)$$

$$ay^2 - 2r_- y + ar_- > 0, \quad \text{for } C_5. \qquad (B45)$$

Since the expressions above have positive quadratic coefficients, the inequalities (B44) and (B45) are satisfied when

$$y < \frac{r_+}{a}(1 - \sqrt{1 - r_-}) \quad \text{or} \quad y > \frac{r_+}{a}(1 + \sqrt{1 - r_-}),$$

$$(B46)$$

for C_4 and

$$y < \frac{r_-}{a}(1 - \sqrt{1 - r_+}) \quad \text{or} \quad y > \frac{r_-}{a}(1 + \sqrt{1 - r_+}),$$

$$(B47)$$

for C_5. In the case of (B47), the radicand $1 - r_+ = -\sqrt{1 - a^2}$ is strictly negative[13] and the roots are complex. The quadratic expression is therefore always positive, and (B43) is always negative. For (B46), we note that since

$$\frac{1 - \sqrt{1 - r_-}}{a} < 1 \quad \text{for} \quad 0 < a < 1,$$

$$(B48)$$

the lower root is subhorizon and thus irrelevant (because $r_u > r_+$). So what we must check is whether we can ever have

$$r_u = y^2 > \frac{r_+^2}{a^2}(1 - \sqrt{1 - r_-})^2.$$

$$(B49)$$

In fact, (B49) is never satisfied for prograde orbits. To see why, recall [28] that for prograde equatorial orbits,

$$r_{\text{isco}} = 3 + Z_2 - [(3 - Z_1)(3 + Z_1 + 2Z_2)]^{1/2},$$

$$Z_1 = 1 + (1 - a^2)^{1/3}[(1 + a)^{1/3} + (1 - a)^{1/3}], \quad (B50)$$

$$Z_2 = (3a^2 + Z_1^2)^{1/2}.$$

A simple plot (not included here) shows that

$$r_{\text{isco}} < \frac{r_+^2}{a^2}(1 - \sqrt{1 - r_-})^2 \quad \text{for } 0 < a < 1.$$

$$(B51)$$

Since $r_u < r_{\text{isco}}$ for all (eccentric) homoclinic orbits, (B49) is never satisfied, and (B42) is always positive. The upshot is that we can write the $C_{4,5}^{(t)}$'s so that every factor outside a radical is positive. Specifically,

$$C_4^{(t)} = -\frac{4r_+}{r_+ - r_-}\sqrt{1 - E^2}\frac{2r_+ r_u^{1/2} \mp a(r_u + r_+)}{\sqrt{r_+[2 - (2r_u + r_+)(1 - E^2)]r_u^{3/2}(r_u^{3/2} - 3r_u^{1/2} \pm 2a)}},$$

$$(B52)$$

$$C_5^{(t)} = -\frac{4r_-}{r_+ - r_-}\sqrt{1 - E^2}\frac{-2r_- r_u^{1/2} \pm a(r_u + r_-)}{\sqrt{r_-[2 - (2r_u + r_-)(1 - E^2)r_u^{3/2}(r_u^{3/2} - 3r_u^{1/2} \pm 2a)}},$$

$$(B53)$$

where we have used Eq. (B29) to rewrite the factors $(r_a - r_\pm)$ in the radicands of the denominators as

$$r_a - r_\pm = \frac{2 - (2r_u + r_\pm)(1 - E^2)}{1 - E^2}.$$

$$(B54)$$

Since the numerators of the factors on the second lines are now manifestly positive, they can be brought under the radical sign without having to worry about stray factors of -1. We are left with

$$C_4^{(t)} = -\frac{4r_+}{r_+ - r_-}\sqrt{1 - E^2}\sqrt{\frac{[2r_+ r_u^{1/2} \mp a(r_u + r_+)]^2}{r_+[2 - (2r_u + r_+)(1 - E^2)]r_u^{3/2}(r_u^{3/2} - 3r_u^{1/2} \pm 2a)}},$$

$$(B55)$$

$$C_5^{(t)} = -\frac{4r_-}{r_+ - r_-}\sqrt{1 - E^2}\sqrt{\frac{[-2r_- r_u^{1/2} \pm a(r_u + r_-)]^2}{r_-[2 - (2r_u + r_-)(1 - E^2)]r_u^{3/2}(r_u^{3/2} - 3r_u^{1/2} \pm 2a)}},$$

$$(B56)$$

Finally, each of the large radicands in (B55) and (B56) is 1. To see this, we use Eq. (A4a) to rewrite the $1 - E^2$ in each denominator as

$$1 - E^2 = \frac{r_u^2 - 4r_u \pm 4ra_u^{1/2} - a^2}{r_u^{3/2}(r_u^{3/2} - 3r_u^{1/2} \pm 2a)}$$

$$(B57)$$

so that distributing the $r_u^{3/2}(r_u^{3/2} - 3r_u^{1/2} \pm 2a)$ in the denominators of the radicands leaves them in the form

$$r_+[2r_u^{3/2}(r_u^{3/2} - 3r_u^{1/2} \pm 2a)$$

$$- (2r_u + r_+)(r_u^2 - 4r_u \pm 4ar_u^{1/2} - a^2)], \quad \text{for } C_4^{(t)}$$

$$(B58)$$

---

[13]For $a = 1$, the radicand is 0, not negative. However, in this scenario, $r_- = 1$ and the quadratic expression in (B45) has a double root at $y = 1 \Rightarrow r_u = 1$. Since $r_u \geq 1$ for all a, then even in the $a = 1$ case, the quadratic in (B45) will be non-negative. Of course, the $a = 1$ case for any analysis of orbital motion must be handled carefully since the r coordinate values of the inner and outer horizons, the itco, the ibco, and the isco are all unphysically degenerate in the maximal spin case.

$$r_-[2r_u^{3/2}(r_u^{3/2} - 3r_u^{1/2} \pm 2a)$$
$$- (2r_u + r_-)(r_u^2 - 4r_u \pm 4ar_u^{1/2} - a^2)], \quad \text{for } C_5^{(t)}.$$
$$(B59)$$

Multiplying out the numerators and denominators and grouping them by powers of r_u then shows that they are identical, for both prograde and retrograde orbits.

The final expressions for the coefficients $C_{4,5}^{(t)}$ are compact. Noting that $r_+ - r_- = 2\sqrt{1 - a^2}$, those expressions are

$$C_4^{(t)} = -\frac{2r_+}{\sqrt{1 - a^2}} \times \sqrt{1 - E^2} \qquad (B60)$$

$$C_5^{(t)} = -\frac{2r_-}{\sqrt{1 - a^2}} \times 2\sqrt{1 - E^2}. \qquad (B61)$$

To get the corresponding φ coefficients, note that

$$2aE - L_z r_\mp = \frac{1}{r_\mp}[2aEr_\pm - L_z \underbrace{r_\mp r_\pm}_{a^2}]$$
$$= \frac{a}{r_\pm}[2Er_\pm - aL_z]. \qquad (B62)$$

Thus,

$$C_4^{(\varphi)} = \frac{1}{2}\frac{a}{r_+}C_4^{(t)} = -\frac{a}{\sqrt{1 - a^2}} \times \sqrt{1 - E^2} \qquad (B63)$$

$$C_5^{(\varphi)} = \frac{1}{2}\frac{a}{r_-}C_5^{(t)} = -\frac{a}{\sqrt{1 - a^2}} \times \sqrt{1 - E^2}. \qquad (B64)$$

To summarize, once simplified, the coefficients in (B26) become

$$C_1^{(\tau)} = 1, \qquad C_2^{(\tau)} = \frac{2}{1 - E^2},$$

$$C_3^{(\tau)} = \frac{2}{\gamma\lambda_r}, \qquad C_1^{(t)} = E,$$

$$C_2^{(t)} = 2E\left(\frac{3 - 2E^2}{1 - E^2}\right), \qquad C_3^{(t)} = \frac{2}{\lambda_r}\sqrt{1 - E^2},$$

$$C_3^{(\varphi)} = 2\frac{\Omega_u}{\lambda_r}\sqrt{1 - E^2}, \qquad C_4^{(t)} = -\frac{2r_+}{\sqrt{1 - a^2}}\sqrt{1 - E^2},$$

$$C_4^{(\varphi)} = -\frac{a}{\sqrt{1 - a^2}}\sqrt{1 - E^2},$$

$$C_5^{(t)} = -\frac{2r_-}{\sqrt{1 - a^2}}\sqrt{1 - E^2},$$

$$C_5^{(\varphi)} = -\frac{a}{\sqrt{1 - a^2}}\sqrt{1 - E^2}. \qquad (B65)$$

5. Analytic expressions for homoclinic orbits

We can now put everything together from the prior subsections. Looking back at Eqs. (B22)–(B24) and substituting from (B25) and (B65), we arrive at the final expressions for all the dynamical variables:

$$\tau(r) = \frac{1}{\sqrt{1 - E^2}}\sqrt{r(r_a - r)} + \frac{2}{(1 - E^2)^{3/2}}\tan^{-1}\sqrt{\frac{r_a - r}{r}}$$
$$+ \frac{2}{\gamma\lambda_r}\tanh^{-1}\sqrt{\frac{r_u}{r_a - r_u}\frac{r_a - r}{r}}, \qquad (B66)$$

$$t(r) = \frac{E}{\sqrt{1 - E^2}}\sqrt{r(r_a - r)} + 2E\frac{(3 - 2E^2)}{(1 - E^2)^{3/2}}\tan^{-1}\sqrt{\frac{r_a - r}{r}}$$
$$+ \frac{2}{\lambda_r}\tanh^{-1}\sqrt{\frac{r_u}{r_a - r_u}\frac{r_a - r}{r}} - \frac{2r_+}{\sqrt{1 - a^2}}$$
$$\times \tanh^{-1}\sqrt{\frac{r_+}{r_a - r_+}\frac{r_a - r}{r}}\frac{2r_-}{\sqrt{1 - a^2}}$$
$$\times \tanh^{-1}\sqrt{\frac{r_-}{r_a - r_-}\frac{r_a - r}{r}}, \qquad (B67)$$

$$\varphi(r) = 2\frac{\Omega_u}{\lambda_r}\tanh^{-1}\sqrt{\frac{r_u}{r_a - r_u}\frac{r_a - r}{r}} - \frac{a}{\sqrt{1 - a^2}}$$
$$\times \tanh^{-1}\sqrt{\frac{r_+}{r_a - r_+}\frac{r_a - r}{r}}\frac{a}{\sqrt{1 - a^2}}$$
$$\times \tanh^{-1}\sqrt{\frac{r_-}{r_a - r_-}\frac{r_a - r}{r}}. \qquad (B68)$$

[1] K. Glampedakis, Classical Quantum Gravity **22**, S605 (2005).

[2] E. E. Flanagan and S. A. Hughes, Phys. Rev. D **57**, 4535 (1998).

[3] K. Glampedakis, S. A. Hughes, and D. Kennefick, Phys. Rev. D **66**, 064005 (2002).

[4] S. Drasco and S. A. Hughes, Phys. Rev. D **69**, 044015 (2004).

[5] S. Drasco, E. E. Flanagan, and S. A. Hughes, Classical Quantum Gravity **22**, S801 (2005).

[6] S. Drasco and S. Hughes, Phys. Rev. D **73**, 024027 (2006).

[7] R. N. Lang and S. A. Hughes, Phys. Rev. D**74**, 122001 (2006).

[8] N. A. Collins and S. A. Hughes, Phys. Rev. D **69**, 124022 (2004).

[9] S. Drasco, Classical Quantum Gravity **23**, S769 (2006).

[10] S. Chandrasekhar, Proc. R. Soc. A **421**, 227 (1989).

[11] J. Levin and G. Perez-Giz, Phys. Rev. D **77**, 103005 (2008).

[12] R. O'Shaughnessy, Phys. Rev. D **67**, 044004 (2003).

[13] K. Glampedakis and D. Kennefick, Phys. Rev. D **66**, 044002 (2002).

[14] J. Levin and R. Grossman, Phys. Rev. D **79**, 043016 (2009).

[15] R. Grossman and J. Levin (unpublished).

[16] G. Perez-Giz and J. Levin, following Article, Phys. Rev. D **79**, 124014 (2009).

[17] U. Sperhake *et al.*, Phys. Rev. D **78**, 064069 (2008).

[18] F. Pretorius and D. Khurana, Classical Quantum Gravity **24**, S83 (2007).

[19] J. Levin, R. O'Reilly, and E. Copeland, Phys. Rev. D **62**, 024023 (2000).

[20] L. Bombelli and E. Calzetta, Classical Quantum Gravity **9**, 2573 (1992).

[21] H. Poincaré, *Méthodes Nouvelles de la Mécanique Céleste* (Gauthier Villars, Paris, 1892).

[22] W. Schmidt, Classical Quantum Gravity **19**, 2743 (2002).

[23] T. Hinderer and E. E. Flanagan (unpublished).

[24] B. Carter, Phys. Rev. **174**, 1559 (1968).

[25] R. Wald, *General Relativity* (University of Chicago Press, Chicago, IL, 1984).

[26] J. Hartle, *Gravity: An Introduction to Einstein's General Relativity* (Addison Wesley, San Francisco, CA, 2003).

[27] S. Chandrasekhar, *The Mathematical Theory of Black Holes* (Clarendon Press, Oxford, 1983).

[28] J. M. Bardeen, W. H. Press, and S. A. Teukolsky, Astrophys. J. **178**, 347 (1972).